*Scientific paper*

# Solvothermal Synthesis and Photocatalytic Activity of BiOBr Microspheres with *Hierarchical* Morphologies

**Adriana C. Mera,[1, 2*] Carlos A. Rodríguez,[1, 2] Héctor Valdés,[3] Andres F. Jaramillo,[4] David Rojas[4] and Manuel F. Meléndrez[4]**

[1] *Instituto de Investigación Multidisplinario en Ciencia y Tecnología, Universidad de La Serena, Benavente 980, La Serena, Chile.*

[2] *Laboratorio de Química Analítica e Investigación en Fotoquímica y Productos Naturales, Departamento de Química, Facultad de Ciencias, Universidad de La Serena, La Serena, Chile.*

[3] *Universidad Católica de la Santísima Concepción, Facultad de Ingeniería, Laboratorio de Tecnologías Limpias, Concepción, Chile.*

[4] *Advanced Nanocomposites Research Group (GINA). Hybrid Materials Laboratory (HML). Department of Materials Engineering (DIMAT), Faculty of Engineering, University of Concepcion, 270 Edmundo Larenas, Box 160-C, Concepcion, Chile 4070409.*

* *Corresponding author: E-mail: adrymera@hotmail.com, amera@userena.cl Phone: +56-51-2334881*

*Received: 10-01-2018*

## Abstract

BiOBr microspheres with hierarchical morphologies (BiOBr-MicSphe) has potential application in heterogeneous photocatalysis for decontamination of water and air. For this reason, the synthesis, characterization an evaluation of photocatalytic activity of these materials become important. In this article, BiOBr-MicSphe were synthesized using different ranges of reaction temperature (120–200 °C) and reaction time (12 h – 24 h). Samples grown at 145 °C and 18 h showed the higher photocatalytic activity on gallic acid degradation. Morphological properties, chemical composition and structural analysis revealed that sample with higher photocatalytic activity exhibited a microspherical morphology with pure BiOBr tetragonal phase. Besides, adsorption-desorption analysis showed a smaller pore diameter for sample grown at 145 °C and 18 hrs. The results showed that the reaction temperature has a strong influence on the different properties of the material, affecting the photocatalytic activity.

**Keywords**: BiOBr MicSphe; solvothermal; properties; photocatalytic activity

## 1. Introduction

Currently, wastewater treatment using new technologies such as advanced oxidation processes (AOP's) for toxic organic removal is under continuous study. The heterogeneous photocatalysis is found among the most promising and efficient AOPs to control environmental pollution, due to its demonstrated efficiency in the degradation and mineralization of a wide range of organic compounds. Heterogeneous photocatalysis is a process based on the utilization of light energy to activate a semiconductor, which modifies the rate of a chemical reaction without being involved itself. The semiconductor can be activated using artificial radiation or solar radiation.[1,2] The most used semiconductor in the industry today is titanium dioxide ($TiO_2$) *Evonik* P-25. It offers the benefits of being inert, inexpensive, stable and non-toxic.[3] However, due to its wide band gap of 3.2 eV, this material can only absorb light energy in the UV region, which is only around a 5% of the solar spectrum. This makes $TiO_2$ relatively unattractive for wastewater treatment, since it cannot be activated by natural solar radiation.[4–6] $TiO_2$ has been modified to be efficient under visible light using different strategies; however, the increases in photocatalytic efficiency is minimum.[7–9] Therefore, nowadays most of research that is conducted in the field of photocatalysis, has moved to the development of new materials that are active under visible light.[10,11]

Recently, the family of bismuth oxyhalides (BiOX, X=Cl, Br, I) has been investigated for their photocatalytic

properties under visible radiation with favorable results.[12] Among them, bismuth oxybromide (BiOBr) has shown promising results.[13,15] BiOBr has exhibited greater photocatalytic activity than the commercialized *Evonik* P25 under UV radiation.[16]

BiOBr have been previously synthetized by several methods, such as hydrolysis, hydrothermal, solvothermal, microwave, microemulsion and ionothermal.[17–23] However, among all available procedures, the solvothermal method appears as one of the most promising, due to the higher photocatalytic activity of the obtained materials.[24]

In recent years, several authors have reported the synthesis of BiOBr microspheres by solvothermal method. In 2008 J. Zang *et. al.*[25] grew BiOBr micropheres at 170 °C and 6 h. Samples showed a visible light induced photocatalytic activity for the degradation of methyl orange (MO). In 2011 J. Xu *et. al.*,[26] using solvothermal method at 180 °C and 12 h, synthesized BiOBr microspheres. The prepared BiOBr catalysts exhibited of pure tetragonal phase, which removed nearly 100 % of RhB from solution after 60 min under simulated solar light irradiation. The high photoactivity was attributed to its relatively large specific surface area and efficient absorption of visible light. Finally, in 2012, Y. Huo *et. al.*,[25] reported the synthesize of BiOBr microspheres at 160 °C and 12 h. The authors determine that the high photocatalytic activity of BiOBr material for rhodamine B (RhB) degradation under visible-light irradiations could be ascribed to the strong light absorbance with the light multi-reflection, the efficient separation of photo-generated electron–hole pairs, the high crystallization and the large surface area.

All these works reported the obtainment of BiOBr microspheres under single conditions; however, the influence of using different temperatures in the solvothermal synthesis on the properties and photocatalytic activity of these materials has not been reported yet. Besides, considering the high photocatalytic activity of BiOBr, it is necessary to standardize the experimental conditions (reaction temperature and reaction time) of solvothermal synthesis, to obtain a reproducible method which enables to extend the synthesis and application to an industrial scale. The interest in using this material is also because it can be obtained in the form of spheres with *Hierarchical* structures. These structures allow the increase of the surface area of the material, increasing the efficiency of the photocatalytic system. In this work, it is further shown that these can be obtained using temperatures below 150 °C.

The aim of this work is to determine the optimum values of temperature and reaction time for the solvothermal synthesis of BiOBr microspheres with *Hierarchical* structures, to obtain the highest photocatalytic activity. The standardization of conditions (temperature and reaction time) were developed using response surface methodology (RSM).[27–32] In addition, the obtained materials from standard conditions were characterized to understand the influence of the temperature and time of solvothermal synthesis, on gallic acid photocatalytic degradation. Gallic acid (model compound) was selected as a representative phenol structure present in agro-industry wastes such as winery wastewaters.[33, 34] This compound is responsible for the inhibitory effects on microbial activity in biological treatment systems, generally used for the treatment of these wastewaters. [35,36]

# 2. Experimental

## 2. 1. Preparation of BiOBr Materials

BiOBr Microspheres (BiOBr-MicSphe) were obtained by solvothermal synthesis. The synthesis of materials was performed using a solution of ethylene glycol (Merck 99.5%) with concentration 0.1 M of KBr (99.0% Merck), was added to a solution of ethylene glycol with concertation 0.1 M of bismuth nitrate pentahydrate ($Bi(NO_3)_3 \times 5H_2O$ (99.0%, Sigma-Aldrich). The mixture was stirred at room temperature and then poured into to an autoclave reactor. The reactor was heated using the experimental design displayed in Table 1. After the reaction times has elapsed, the reactor is cooled down at room temperature, for each experiment. The solids were separated by gravity filtration and washed with distilled absolute ethanol and water. The BiOBr materials obtained were dried at 60 °C for 24 hours.

## 2. 2. Response Surface Modeling

The solvothermal synthesis of BiOBr was carried out with the response surface methodology (RSM) using the software MODDE 7.[37–40] The multivariate analysis was a composed central circumscribed design (CCC) which is based on a factorial design of two level with 3 central points and 4-star points.[27–32] The central point was coded as zero and determined in triplicate to statistically validate the determinations assuming homoscedasticity of variance.

The variables evaluated simultaneously were the temperature (ranging from 120 to 200 °C) and reaction time (from 12 to 24 hours). This procedure allows standardization of the experimental conditions (reaction time and reaction temperature) for the synthesis of BiOBr microspheres by solvothermal process. The statistical validation was performed by ANOVA test with a confidence level of 95%.

## 2. 3. Characterization

The materials that exhibited the higher and lower photocatalytic efficiency were selected for characterization further. The morphologies of materials were observed by scanning electron microscopy (SEM, JEOL JSM-6380). Additionally, transmission electron microscopy (TEM) using a JEOL JEM 1200 EX-II. The particles size were determined by using a laser diffraction particle size analyzer

(Microtrac Model S3500). Chemical composition of the samples was measured by means of energy dispersive X-ray spectroscopy (EDS). Micromeritis TriStar II porosity analyzer measured the specific surface area (BET) and the pore size distribution of the materials. The composition of products was examined by means of X-ray diffraction (XRD) in a diffractometer Bruker D4 with X-ray source of Cu Kα (λ = 1.5406 A). Thermogravimetric measurement (TGA) were determined with a thermobalance model TG209 F1 Iris. Fourier transform infrared (FTIR) spectra were obtained using a Nicolet Nexeus spectrometer. UV-visible diffuse reflectance absorbance (DRS) was determined with a Perkin Elmer Precisely Lambda 35 UV/Vis spectrophotometer.

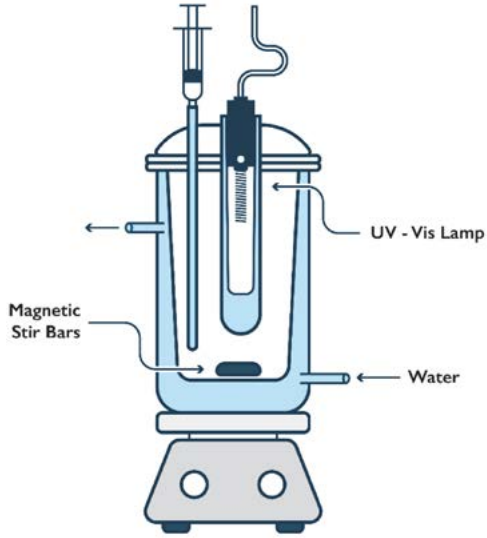


**Figure 1.** Experimental system used during the photocatalytic assays.

## 2. 4. Photocatalytic Efficiency Measurements

The photocatalytic efficiency was evaluated on gallic acid degradation under simulated solar radiation using a xenon lamp (VIPHID 6000 k, 12 W) with spectral range between 380–900 nm.[41] The tests were made in the system of Figure 1, the photocatalytic assays were done in 250 mL of acid gallic aqueous solution (20 mg $L^{-1}$) adding 0.025 g of the photocatalyst. The reaction mixture was maintained at room temperature and the pH was fixed at 4.5. Before the light was turned on, the solution was kept in dark for 40 min to reach the absorption-desorption equilibrium. Subsequently, solution was irradiated during 60 min and sampling was done every 5 min until 20 min, then every 10 min to complete the 60 min of photocatalytic reaction.[31] Remaining gallic acid was determined by absorption measurements at 264.5 nm by means of UV-vis spectrophotometry (Shimadzu UV-1601PC). From the photocatalytic activity measurements samples that exhibited the higher and lower activity were selected for further characterization.

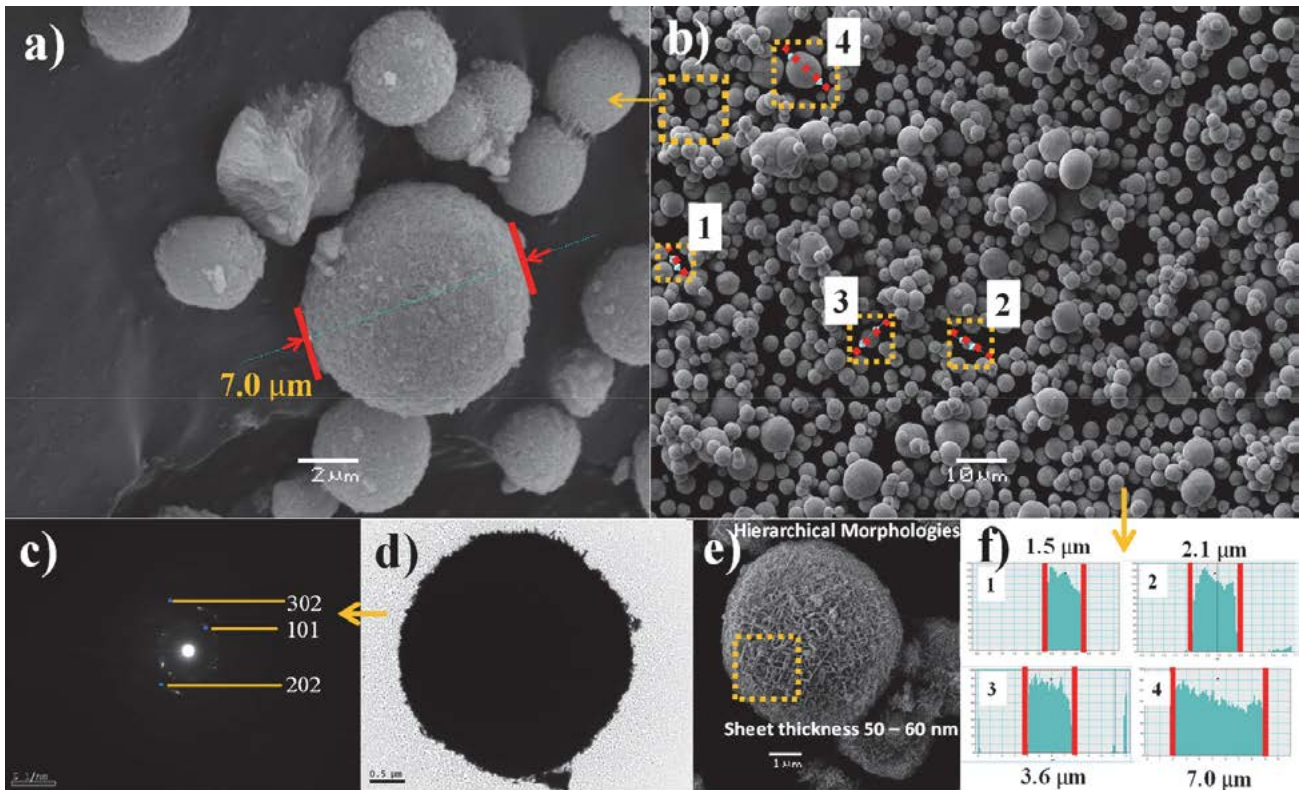


**Figure 2.** SEM and TEM images of BiOBr obtained for 18 h and 145 °C

# 3. Results and Discussion

## 3. 1. Characterization of (BiOBr-MicSphe)

The SEM and TEM analyzes of the BiOBr-MicSphe are shown in Figure 2. The spheres shown correspond to those obtained at a lower temperature (145 °C). The synthesis method used to obtain this type of material is efficient and does not produce another type of morphology different to the spherical one, as shown in the microscopy of Fig. 2a and Fig.2b. BiOBr-MicSphe diameter varied from 7.0 to 1.5 μm (Fig. 2f) and its consistency in the interior is completely porous (Fig. 2a). It is important to mention that, a smaller particle size promotes separation and migration of the photogenerated electron-hole pairs, improving the photocatalytic activity.[42]

All the synthesized spheres presented hierarchical structures composed of sheets that are interlaced in inside, generating a structure highly porous and with greater surface area in comparison to smooth structures. On the other hand, an analysis of SEAD (selected area electron diffraction) of the sphere shown in Fig. 2d was performed. The diffraction pattern (Fig. 2c) showed the following crystalline planes (101), (202) and (303), characteristic to phases corresponding to BiOBr. Other phases were not found in the analyzes so it is concluded that all the spheres are constituted BiOBr tetragonal type. The above argument is reinforced with the XRD analyzes (Fig. 3) where the phases found for the spheres obtained at 145 °C correspond to tetragonal BiOBr.

The XRD pattern of the BiOBr-MicSphe synthetized at 145 °C and 217 °C, are shown in las Fig. 3a and Fig. 3b, respectively. BiOBr synthetized at 145 °C, exhibited tetragonal structure according to the reference JCPDS Card 01-078-0348. No impurity peaks or presences of other phases were observed. In contrast, BiOBr-MicSphe synthesized at 217 °C shows a mixture of two phases. The first one corresponding to the tetragonal BiOBr (JCPDS Card: 01-078-0348), and the second one ascribed to the cubic phase of $Bi_2O_3$ (JCPDS Card: 01-077-0374). From the XRD pattern, the average size of crystallite (D) can be estimated by using the Scherrer's equation as follows:[43]

$$D=\frac{K\lambda}{\beta \cos \Theta} \quad (1)$$

where λ is the wavelength of X-ray radiation (λ = 0.15406 nm, for copper), *K* is the Scherrer's constant (*K* = 0.94), $\theta$ is the Bragg angle, $\beta$ is the half width full maximum of the peak.[42] The average crystal size for samples grown at 145 °C and 217 °C were 14.2 nm and 40.7 nm, respectively. The observed difference in the crystallite sizes, is a consequence of the different applied temperature during the growth process, since it is well-known that higher temperatures result in bigger crystal size.

The presence of $Bi_2O_3$ can be a consequence of the increased temperature during the BiOBr fabrication process. The solvent of the reactants is ethylene glycol which is

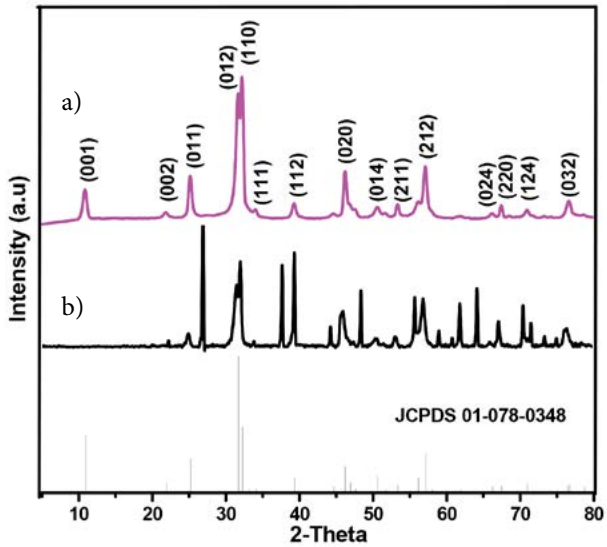


**Figure 3.** XRD patterns and BiOBr obtained for 18 h at **a)** 145 °C and **b)** 217 °C.

a coordinator agent that prevents premature hydrolysis of bismuth nitrate in nitric acid in the solvothermal synthesis of BiOBr (Eq. 2).[30]

$$2Bi(NO_3)_3 \cdot 5H_2O+3HOCH_2CH_2OH \rightarrow Bi_2(OCH_2CH_2O)_3+6HNO_3+10H_2O \quad (2)$$

At low temperature, reacts slowly with water and bromide, forming the BiOBr and releasing the ethylene glycol (Eq. 3).

$$Bi_2(OCH_2CH_2O)_3+H_2O+KBr \rightarrow BiOBr+HOCH_2CH_2OH \quad (3)$$

whenever the temperature increases in autoclave conditions, nitric acid dissociates and acts as a strong oxidizing agent, consuming halides, and transforming the $Br^{-1}$ in $Br_2$ (Eqs. 4 and 5):

$$4HNO_3 \rightarrow 2H_2O+4NO^{3-}+3O_2 \quad (4)$$

$$8H^{+}+2NO^{3-}+6Br^{-} \rightarrow 3Br_2+2NO+4H_2O \quad (5)$$

Equation 3, shows that the reaction releases $H^+$ ions, whereas that in Eqs. 4 and 5 the reactions consume $H^+$. Some works have reported that under acid condition the synthesis of BiOBr is favorable, whereas to basic pH BiOBr materials are poor in halogen.[44] Thus, as the temperature rises the pH increases favoring the formation of $Br_2$ and leading to less bromide ions ($Br^-$) ions available. In this way, once bromide ions are consumed, $Bi^{3+}$ reacts with $O_2$ to form $Bi_2O_3$.This information is supported by the qualitative analysis of chemical composition by EDS (supplementary material (Fig.S1)).

On the other hand, Figure 4 shows the thermograms of BiOBr obtained at 145 °C and 217 °C of the materials that

shown the higher and the lower photocatalytic activity, respectively. It can be clearly seen a loss of weight in a multistage process, where the decomposed products are not stable intermediates for both cases. Both thermograms show that the materials suffer weight loss during the analysis. Between 40 to 300 °C, no significant decrease in weight is observed (about 5%), which is associated with the loss of water of hydration.

It can be seen from the curve corresponding to BiOBr obtained at 145 °C (Fig. 4a), that close to 600 °C the material has a first significant weight loss, which may be generated by the thermal decomposition of the microspheres monoxide bismuth (BIO) and $Br_2$ (Eq. 6)

The second and last significant weight loss of this material occurs at 900 °C, which may be ascribed to the decomposition of BiO in $Bi_2O_3$ and metallic bismuth (Eq. 7). A total reduction of 46% of weight is observed from 300 °C to 900 °C.[46–50]

$$2BiOBr \rightarrow 2BiO + Br_2 \quad (6)$$

$$3BiO \rightarrow Bi_2O_3 + Bi \quad (7)$$

In the case of sample obtained at 217 °C (Fig. 4b), weight loss starts at 400 °C and only a 35% of weight reduction is observed at 900 °C. These results show that BiOBr synthesized at 217 °C could be more thermally stable than the material synthesized at 145 °C. This higher thermal stability exhibited by BiOBr synthesized at 217 °C is a consequence of the presence of $Bi_2O_3$, which is known to be more stable for a wide range of temperatures.[46,47]

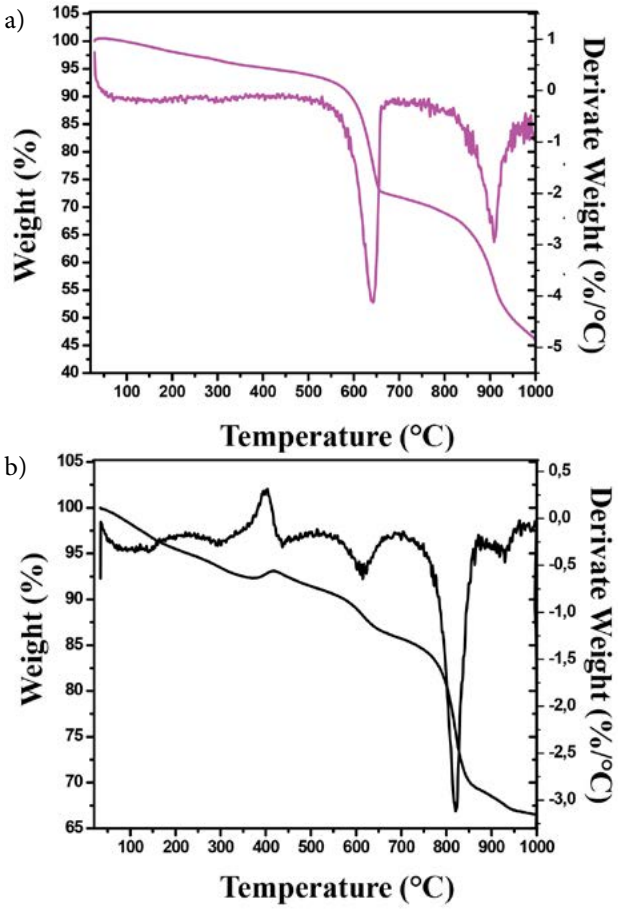


**Figure 4.** TGA-DTA profile of BiOBr obtained for 18 h at **a)** 145 °C and **b)** 217 °C.

The BJH isotherm of the materials synthesized at 145 °C and 217 °C are shown in Fig. 5. The sample obtained at 145 °C exhibit irreversible type IV adsorption isotherms with an H3 hysteresis loop confirming the mesopore structure.[48] In addition, pore size distribution is around 14 nm, as shown in Fig. 5a (inset). In contrast, the material synthesized at 217 °C exhibits a type II isotherm characteristic of a non-porous material, this material does not exhibit a porous morphology (Fig. 5b).

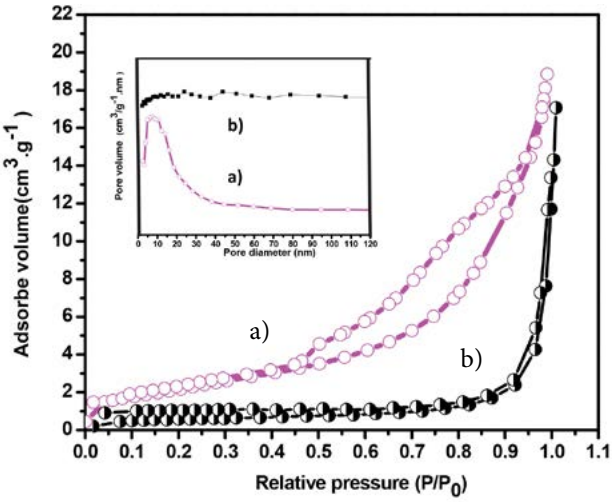


**Figure 5**. adsorption-desorption isotherms of BiOBr obtained for 18 h at **a)** 145 °C and **b)** 217 °C.

Table 1 shows the average values of textural properties of the synthesized materials obtained at different reaction temperatures, determined by nitrogen adsorption at 77 K. The higher value of surface is in relation with the high catalytic activity showed by BiOBr material with microspheres morphology, since it is known that higher surface area favors the catalytic activity.[49]

**Table 1:** Values of textural properties of BiOBr materials prepared at 18 h reaction using 145 °C and 217 °C, respectively.

| Temperature °C | BET $m^2/g$ | Pore diameter (nm) | Pore Volume ($cm^3/g$) |
|---|---|---|---|
| 145 | 19 | 14 | 0,05 |
| 217 | 3 | 60 | 0,05 |

Figures 6a and 6b show the FTIR spectra of BiOBr-MicSphe synthesized at 145 °C and 217 °C, respectively. Spectrum of pure BiOBr microspheres (material obtained at 145 °C), exhibits two bands around 3500 and 1600 $cm^{-1}$, which are attributed to OH symmetrical stretching and

scissoring vibrations, due to adsorbed water.[50,51] The absorption bands located at 512 $cm^{-1}$ and 770 $cm^{-1}$ are ascribed to the stretching vibrations of Bi-O (Fig. 5a). Signals registered in the infrared middle and far away from the BiOX, are in accordance with those reported in the literature for this type of materials.[52] However, from spectrum corresponding of material synthesized at 217 °C, no peaks in the region between 3500 and 1600 $cm^{-1}$ are observed (Fig. 5b). Is possible that the OH bonds suffer rupture such as consequence of high temperature.

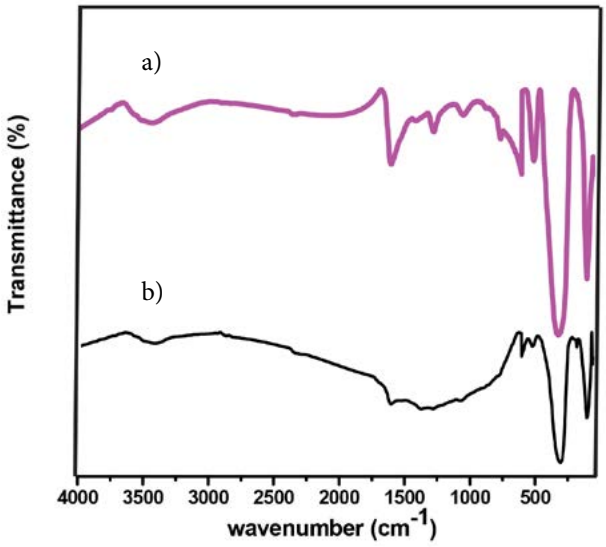


**Figure 6.** FTIR spectra of BiOBr obtained for 18 h at **a)** 145 °C and **b)** 217 °C.

The optical properties of the BiOBr-MicSphe synthetized at 145 °C and 217 °C were studied using diffuse reflectance spectroscopy (DRS) in the UV–vis range. Fig. 7 shows the DRS curves of the BiOBr obtained to different temperatures, from which the band gap were determined.

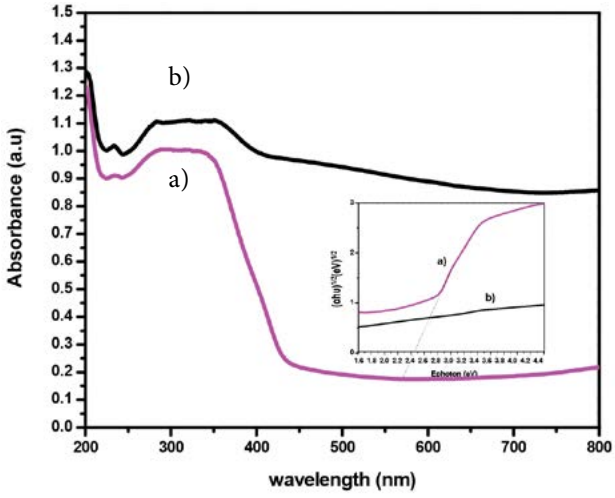


**Figure 7.** UV–Vis diffuse reflectance spectra (DRS) of BiOBr obtained for 18 h at **a)** 145 °C and **b)** 217 °C

The $E_g$ of the materials were calculated by the Tauc representation, using the Eq. 8.

$$\alpha(h\nu)=A\cdot(h\nu-E_g)^{n/2} \quad (8)$$

Where α is the absorption coefficient, h is the Planck constant, ν is the light frequency, $E_g$ is the band gap energy, and n is related to semiconductor transition (n = 4 for BiOBr.[53–54] The inset in Fig. 7 allows the determination of the band gap directly from extrapolation in the Tauc plot. The values found were 2.88 ± 0.01 eV and 2.48 ± 0.01 eV for materials obtained at 145 °C and 217 °C, respectively. These values are in good agreement with those reported previously by several authors for BiOBr microspheres.[54–55] The lower band gap of the sample grown at 217 °C could be a consequence of the increased crystal size of BiOBr.[56]

In addition, the band-edge position of BiOBr can be estimated by using the following empirical equations.[43,51]

$$E_{VB}=X-E^e+0.5\times E_g \quad (9)$$

$$E_{CB}=E_{VB}-E_g \quad (10)$$

Where $E_{VB}$ is the valence band potential (VB) edge, $E_{CB}$ is the conduction band potential (CB) edge, X is the electronegativity of the semiconductor (6.17 eV for BiOBr,[53] $E^e$ is the energy of free electron on the hydrogen scale (about 4.5 eV), and $E_g$ is the band gap energy of the semiconductor. Accordingly, $E_{VB}$ and $E_{CB}$ were calculated to be 3.11 ± 0.01 eV and 0.23 ± 0.02 eV for BiOBr grown at 145 °C, and 2.91 ± 0.01 eV and 0.43 ± 0.02 eV for BiOBr synthesized at 217 °C. These values agree with those reported by other authors.[57–58] These parameters are very important to identify the reactive species in the photocatalytic reaction.[59]

## 3. 2. Photocatalytic Efficiency

The 11 experiments performed to obtain the different BiOBr-MicSphe samples by simultaneously varying the temperature and the reaction times in the autoclave reactor are shown in Table 2.

The rate constants were used as response factor (Y); these constants are shown in Table 3 and were calculated considering that reaction kinetics gallic acid degradation follows a pseudo first-order reaction model as expressed in Eq. 11.[60–61] The reaction order is assumed in catalytic processes when the initial pollutant concentration is low.[62]

$$\ln\left(\frac{C_0}{C_t}\right)=kt \quad (11)$$

Where $C_0$ and $C_t$ are the concentration of gallic acid in solution at time 0 and t, respectively, and k is the apparent first-order rate constant.

The polynomial shown in the Eq. 2 obtained by linear regression, represents the weight of the variables, reac-

**Table 1:** Experimental design and results of the rate constants calculated for each trial.

| *Experiment* | Time hours | Temperature °C | Y exp. k (s–1) | Y calc. k (s–1) | % Degradation Experimental |
|---|---|---|---|---|---|
| 1 | 12 (–1) | 120 (–1) | $4{,}30 \times 10^{-5}$ | $4{,}53 \times 10^{-5}$ | 37,7 |
| 2 | 24 (1) | 120 (–1) | $4{,}00 \times 10^{-5}$ | $4{,}33 \times 10^{-5}$ | 43,2 |
| 3 | 12 (–1) | 200 (1) | $3{,}70 \times 10^{-5}$ | $3{,}34 \times 10^{-5}$ | 32,5 |
| 4 | 24 (1) | 200 (1) | $3{,}10 \times 10^{-5}$ | $3{,}15 \times 10^{-5}$ | 37,6 |
| 5 | 9,52 (–√ 2) | 160 (0) | $4{,}00 \times 10^{-5}$ | $4{,}13 \times 10^{-5}$ | 39,2 |
| 6 | 24,5 (√ 2) | 160 (0) | $4{,}10 \times 10^{-5}$ | $4{,}41 \times 10^{-5}$ | 32,8 |
| 7 | 18 (0) | 103,4 (–√ 2) | $4{,}90 \times 10^{-5}$ | $4{,}53 \times 10^{-5}$ | 27,9 |
| 8 | 18 (0) | 216,6 (√ 2) | $2{,}60 \times 10^{-5}$ | $2{,}84 \times 10^{-5}$ | 14,7 |
| 9 | 18 (0) | 160 (0) | $4{,}80 \times 10^{-5}$ | $5{,}27 \times 10^{-5}$ | 43,9 |
| 10 | 18 (0) | 160 (0) | $5{,}10 \times 10^{-5}$ | $5{,}27 \times 10^{-5}$ | 42,5 |
| 11 | 18 (0) | 160 (0) | $5{,}90 \times 10^{-5}$ | $5{,}27 \times 10^{-5}$ | 44,6 |

**Table 3:** Photocatalytic activity of synthesized BiOBr materials prepared at 18 h reaction using 145 °C and 217 °C, respectively.

| Temperature °C | Yield [a] (%) | experimental $k$ [$s^{-1}$] | Gallic acid[b] degradation (%) |
|---|---|---|---|
| 145 | 50 | $6{,}00 \times 10^{-5}$ | 48,2 |
| 217 | 20 | $2{,}84 \times 10^{-5}$ | 14,7 |

[a] Calculated considering the theoretical yield
[b] After 60 min irradiation

tion time (t) and temperature (T) on the gallic acid degradation pseudo first order constant (Y). The validation of the model was performed using the ANOVA test. The values in parentheses in the response polynomial represent the standard deviation of each encoded coefficient. The model proposed in this study has an adequate correlation coefficient ($R^2$ = 0.859) and cross validation correlation coefficient ($Q^2$ = 0.618), values which validated the proposed model.[29]

$$\begin{aligned} Y(k\ BiOBr) = {} & 5.27 \times 10^{-5} (\pm 2.60 \times 10^{-6}) - 9.48 \\ & \times 10^{-7}(t) (\pm 1.59 \times 10^{-6}) - 5.94 \times 10^{-6} (T) \\ & (\pm 1.59 \times 10^{-6}) - 6.39 \times 10^{-6} (t)^2 (\pm 1.90 \times 10^{-6}) \\ & - 7.90 \times 10^{-6} (T)^2 (\pm 1.90 \times 10^{-6}) \end{aligned} \quad (12)$$

The Eq. 12 clearly shows that the most important variable in the solvothermal synthesis of BiOBr microspheres is the temperature, which normally exhibits a negative influence on the photocatalytic activity of the materials when it increases. Meanwhile, the reaction time has weak positive influence. A 3-D representation of response surface of the polynomial is shown in Fig. 8, where a noticeable maximum in the temperature axis is observed, indicating the optimum value of this variable to get the more active catalyst. In this case, the best conditions to obtain the most active catalyst are temperature of 145 °C and 18 h of reaction time.

Fig. 9, shows the correlation of photocatalytic degradation percentages on gallic acid with experimental conditions. Table 2 shown the results of the higher and lower

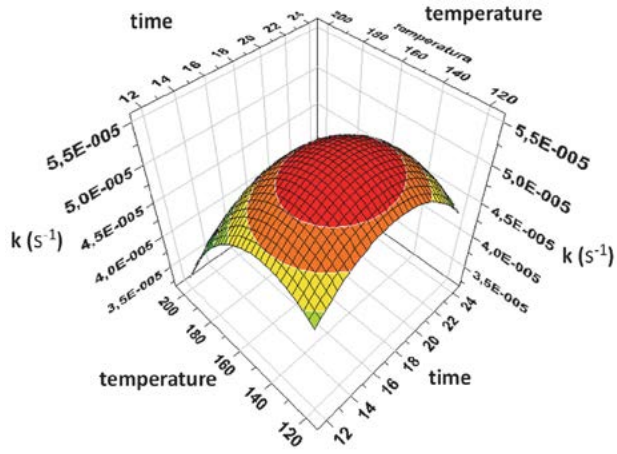


**Figure 8.** 3-D representation of response surface of the polynomial response.

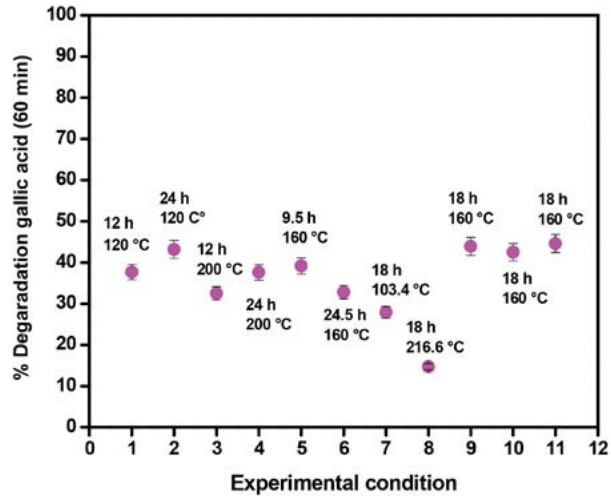


**Figure 9.** Correlation of photocatalytic degradation percentages on gallic acid with experimental conditions of table 2.

photocatalytic efficiency, measured as first order rate constant of gallic acid degradation and degradation percentages.

## 4. Conclusions

In this work, BiOBr microspheres were synthesized by solvothermal process under standardized conditions by controlling the reaction temperature and reaction time. The reaction temperature of 145 °C and time 18 hours, were established as the more appropriate values to obtain BiOBr with microspheres morphology and higher photocatalytic activity on degradation of gallic acid.

In addition, it was determined that the crystalline phase, chemistry composition, morphology, surface area, and size particle of these materials are strongly influenced by the reaction temperature variable, affecting thus directly the photocatalytic activity of these materials. Finally, from the characterization it is possible to conclude that BiOBr samples synthetized using the reported conditions here, are an appropriate material as a photocatalyst for gallic acid degradation under visible light.

## 5. Acknowledgements

This study was funded by Institutional Improvement Plan in Energy Efficiency and Environmental Sustainability (*Plan de Mejoramiento Institucional en Eficiencia Energética y Sustentabilidad Ambiental*) – Project Grant # PMI ULS 1401 of *Universidad de La Serena*.

## 6. References

1. F. Arsac, D. Bianchi, J. Chovelon, P. Conchon, C. Ferronato, A. Lair, M. Sleiman, Mater. *Sci. Eng. C*. **2008**, *28*,722–725. **DOI:**10.1016/j.msec.2007.10.053
2. J. Herrmann, *Catalysis Today*.**1990**, *53*,115–129. **DOI:**10.1016/S0920-5861(99)00107-8
3. U. Gaya, A. Abdullah, *J. Photochem. Photobiol C.* **2008**, 9, 1–12. **DOI:**10.1016/j.jphotochemrev.2007.12.003
4. A. Alinsafia, E. Abdulkarima, M.Ponsa , O. Zahraa, A. Benhammou, A. Yaacoubi, A. Nejmeddine, *Dyes Pigm*. **2017**, *74*, 439–445. **DOI:**10.1016/j.dyepig.2006.02.024
5. Y. Lan, Y. Lu, Z. Ren, *Nano Energy*. **2013**, *2*, 1031–1045. **DOI:**10.1016/j.nanoen.2013.04.002
6. M. Henderson, *Surface Science Report*. **2011**, *66*, 185–297. **DOI:**10.1016/j.surfrep.2011.01.001
7. S. Malato, M. Maldonado, J. Blanco, W. Gernjak, *Catalysis Today*. **2009**, *147*, 1–59. **DOI:**10.1016/j.cattod.2009.06.018
8. Z. Wang, W. Ma, J. Zao: Sensitization of Titania Semiconductor: A Promising Strategy to Utilize Visible Light, en: Phtocatalysis and Water Purification from Fundamentals to Recent Applications, Wiley-VCH, Germany, **2018**, pp.199–231.
9. M. Pelaez, N. Nolan, S. Pillai, M. Seery, P. Falaras, A. Kontos, P. Dunlop, J. Hamilton, J. Byrne, K. O'Shea, M. Entezari, D. Dionysiou D, *Applied Catalysis B*. **2012**, *125*, 331–349. **DOI:**10.1016/j.apcatb.2012.05.036
10. A. Di Paola, E. García, G. Marcì, L. Palmisano, *J. Hazard. Mater.* **2012**, *211–212*, 3–29. **DOI:**10.1016/j.jhazmat.2011.11.050
11. C. Li , Z. Qiang , L. Wenhua, Y. Shuangfeng, *Prog Chem*. **2010**, *22*, 2282–2289.
12. S. R. Zhu, M. K. Wu, W. N. Zhao, F.-Y Yi, K. Tao, L. Han, *J. Solid State Chem.* **2017**, *255*, 17–26. **DOI:**10.1016/j.jssc.2017.07.038
13. H. An, Y. Du, T. Wang, C. Wang, W. Hao, J. Zhang, *Rare Metals*. **2017**, *27*,243–251. **DOI:**10.1016/S1001-0521(08)60123-0
14. X. Zhang, Z. Ai, F. Jia, L. Zhang, *Journal Phys. Chem. C*. **2008**, *112*, 747–753. **DOI:**10.1021/jp077471t
15. S. R. Zhu, Q. Qi, W. N Zhao, M. K. Wu, Y. Fang, K. Tao, F .Y. Yi, L. Han, *Dalton Trans*. **2017**, *46*, 11451–11458. **DOI:**10.1039/C7DT01581J
16. J. Zhang, F. Shi, J. Lin, D. Chen, J. Gao, Z. Huang, X. Ding, C. Tang C, *Chem. Mater.* **2008**, *20*, 2937–2941. **DOI:**10.1021/cm7031898
17. Z. Jiang, F. Yang, G. vYang, L. Kong, M. O. Jones, T. Xiao, P. P. Edwards, *J. Photochem. Photobiol. A*. **2010**, *212*, 8 –13. **DOI:**10.1016/j.jphotochem.2010.03.004
18. H. Deng, J. Wang, Q. Peng, X. Wang, Y. Li, *Chem. Eur. J.* **2005**, *11*, 6519–6524. **DOI:**10.1002/chem.200500540
19. M. Shang, W. Wang, L. Zhang, *J. Hazard. Mater.* **2009**, *167*, 803–809. **DOI:**10.1016/j.jhazmat.2009.01.053
20. L. Zhang, X. Cao, X. Chen, Z. Xue, *J. Colloid Interf. Sci.* **2011**, *354*,630 –636. **DOI:**10.1016/j.jcis.2010.11.042
21. S. R. Zhu, M. K Wu, W. N. Zhao, P. F. Liu, F. Yi, G. Li, K. Tao, L. Han, *Cryst. Growth Des*. **2017**, *17*, 2309–2313. **DOI:**10.1021/acs.cgd.6b01811
22. J. Wang, Y. Li, *Chem. Commun.* **2003**, *18*, 2320–2321. **DOI:**10.1039/b306189b
23. Y. Chen, M. Wen, Q. Wu, *Cryst. Eng. Comm.* **2011**, *13*, 3035–3039. **DOI:**10.1039/c0ce00955e
24. H. Cheng, B. Huang, Z. Wang, X. Qin, *Chem. Eur. J.* **2011**, *17*, 8039 – 8043. **DOI:**10.1002/chem.201100564
25. J. Zhang, F. Shi, J. Lin, D. Chen, J. Gao, Z. Huang, X. Ding, C. Tang, *Chem. Mater.* **2008**, *20*, 2937–2941. **DOI:**10.1021/cm7031898
26. J. Xu, W. Meng, Y. Zhang, L. Li, C. Guo, *Applied Catalysis B*. **2011**, *107*, 355– 362. **DOI:**10.1016/j.apcatb.2011.07.036
27. Y. Huo, J. Zhang, M. Miao, Y. Jin, *Applied Catalysis B*. **2012**, 111–112, 334–341.
28. Z. Šumić, A. Vakula, A. Tepić, J. Čakarević, J. Vitas, B. Pavlić, *Food Chemistry*. **2016**, *203*, 465–475. **DOI:**10.1016/j.foodchem.2016.02.109
29. Contreras D, Freer J, Rodríguez, *J, Inter. Biodeter. Biodegr.* **2006**, *57*, 63–68.
30. D. Contreras, Y. Moreno, Y. Salgado, G. Cardenas, R. Baggio, O. Peña, J. Pivan, *New J. Chem.* **2017**, *31*, 1751–1754. **DOI:**10.1039/b703592f
31. T. Lundstedt, E. Seifert, L. Abramo, B. Thelin, A. Nyström, J. Pettersen, R. Bergman, *Chemometrics Intell. Lab. Syst.* **1989**, *42*, 3–40. **DOI:**10.1016/S0169-7439(98)00065-3
32. A. Mera, C. Rodríguez, M.F. Meléndrez, H. Valdés, *J. Mater. Sci.* **2017**, *52*, 944–954. **DOI:**10.1007/s10853-016-0390-x
33. A. Mera, D. Contreras, N. Escalona, H. Mansilla, *J. Photo-*

*chem. Photobiol. A*. **2016**, *318*,71–76. **DOI:**10.1016/j.jphotochem.2015.12.005
34. F. Beltrán, O. Gimeno, F. Rivas, M. Carbajo, *J. Chem. Tech. Biotechnol*. **2006**, *81*, 1787–1796. **DOI:**10.1002/jctb.1605
35. M. Arienzo, E. Christen, W. Quayle W, *J. Hazard. Mater*. **2009**, *169*, 94–9. **DOI:**10.1016/j.jhazmat.2009.03.069
36. M. Petruccioli, J. Duarte, F. Federici, *J. Biosci. Bioengineering.* **2002**, *90*,381–386. **DOI:**10.1016/S1389-1723(01)80005-0
37. M. Akassou, A. Kaanane, A. Crolla, C. Kinsley, *Water Sci. Technol.* **2010**, *62*,475–83. **DOI:**10.2166/wst.2010.235
38. J. Fernández, J. kiwi, C. Lizama, J. Freer, J. Baeza, H. Mansilla, *J. Photochem. Photobiol.* A Chem. **2012**, *151*, 213–219. **DOI:**10.1016/S1010-6030(02)00153-3
39. C. Lizama, J. Freer, J. Baeza , H. Mansilla H, *Catalysis Today.* **2002**, *76*, 235–246. **DOI:**10.1016/S0920-5861(02)00222-5
40. F. Torrades, M. Pérez, H. Mansilla, J. Peral, *Chemosphere.* **2013**, *53*,1211–1220. **DOI:**10.1016/S0045-6535(03)00579-4
41. M. Pérez, M. Graells, L. J. Del Valle, E. Centelles, H. Mansilla, *Catalysis Today*. **2017**, *124*,163–171. **DOI:**10.1016/j.cattod.2007.03.034
42. B. Leckner, *Sol. Energy*. 1978, *20*, 143–150. **DOI:**10.1016/0038-092X(78)90187-1
43. A. Mera, Y. Moreno, J. Pivan, O. Peña, H. Mansilla*, J. Photochem. Photobiol. A Chem.* **2014**, *289*, 7–13. **DOI:**10.1016/j.jphotochem.2014.05.015
44. D. Smilgies, *J. Appl. Crystallogr*. **2009**, *42*, 1030–1034. **DOI:**10.1107/S0021889809040126
45. Y. Guan, H. Qian, J. Guo J, Yang S, Wang X, Wang S, Fu Y, *Appl. Clay Sci.* **2015**, *114,*124–132. **DOI:**10.1016/j.clay.2015.05.017
46. X. Xiao, R. Hu, C. Liu, C. Xing, X. Zuo, J. Nan, L. Wang, *Chem. Eng. J.* **2013**, *225*,790–797. **DOI:**10.1016/j.cej.2013.03.103
47. J. Song, C. Mao, H. Niu, Y. Shen, S. Zhang, *Cryst. Eng. Comm.* **2010**, *12*, 3875–3881. **DOI:**10.1039/c003497p
48. J. Tóth, *Colloids Surf.* **1990**, *49*,57–69. **DOI:**10.1016/0166-6622(90)80092-I
49. C. Yu, W. Zhou, H. Liu, Y. Li, D. Dionysiou, *Chem. Eng. J.* **2016**. *287*,117–129. **DOI:**10.1016/j.cej.2015.10.112
50. Z. Liu, X. Xu, J. Fang, X. Zhu, J. Chu, B. Li, *Appl. Surf. Sci.* **2012**, *258*, 3771–3778. **DOI:**10.1016/j.apsusc.2011.12.025
51. Z. Liu, B. Wu, Y. Zhu, D. Yin, L. Wang, *Catal. Lett.* **2012**, *142*, 1489–1497. **DOI:**10.1007/s10562-012-0899-9
52. J. Cao, X. Li, H. Lin, S. Chen, X. Fu, *J. Hazard. Mater.* **2012***, 239–240*, 316–324. **DOI:**10.1016/j.jhazmat.2012.08.078
53. Z. Liu, X. Xua, J. Fang, X. Zhua, J. Chua, B. Li, *Appl. Surf. Sci.* **2012**, *258*, 3771–3778. **DOI:**10.1016/j.apsusc.2011.12.025
54. J. Tauc, R. Grigorovici, A. Vancu, *Phys. Stat. Solid B*. **1966**, *15*,627. **DOI:**10.1002/pssb.19660150224
55. D. Wood D, J. Tauc, *Phys. Rev. B*. **1972**, *5*, 3144.
56. X. Xion, L. Ding, Q. Wang, Y. Li, Q. Jiang, J. Hu, *Appl. Catalysis B*. **2016**, *188*,283–291. **DOI:**10.1016/j.apcatb.2016.02.018
57. C. Rodríguez, M. Sandoval, G. Cabello, M. Flores, H. Fernández, C. Carrasco C*, Mater. Res. Bul.* **2014**. *60*, 313–321. **DOI:**10.1016/j.materresbull.2014.08.047
58. P. Wang, P. Yang, Y. Bai, T. Chen, X. Shi, Y. Ye, X. Zhang, *J. Taiwan Ins. Chem. Eng.* **2016**, *68*, 295–300. **DOI:**10.1016/j.jtice.2016.09.013
59. J. Luo, X. Zhou, L. Ma, X. Xu, *J. Molecular Catalysis A Chem.* **2015**, *410*, 168–176. **DOI:**10.1016/j.molcata.2015.09.019
60. A. Kontos, I. Arabatzis, D. Tsoukleris, M. Bernard, D. Petrakis, P. Falaras, *Catalysis Today*. **2015**, *101,* 275–281. **DOI:**10.1016/j.cattod.2005.03.003
61. J. Herrmann, *Catalysis Today*. **1999**, *53*, 115–129. **DOI:**10.1016/S0920-5861(99)00107-8
62. H. Pardue. *Anal. Chim. Acta.* **1989**, *216*, 69–107. **DOI:**10.1016/S0003-2670(00)82005-X

## Povzetek

Mikrosfere BiOBr s hierarhično morfologijo (BiOBr-MicSphe) imajo potencialno uporabo v heterogeni fotokatalizi v procesih dekontaminacije vode in zraka. Zaradi tega je sinteza, karakterizacija in vrednotenje fotokatalitske aktivnosti teh materialov postala pomembna. V članku poročamo o sintezi mikrosfer BiOBr pri kateri smo uporabljali različne razpone reakcijskih temperatur (120–200 °C) in reakcijskega časa (12 h – 24 h). Vzorci, pripravljeni pri 145 °C in 18 h, so pokazali višjo fotokatalitsko aktivnost pri degradaciji galske kisline. Morfološke lastnosti, kemična sestava in strukturna analiza so pokazali, da je imel vzorec z višjo fotokatalitsko aktivnostjo mikrosferično morfologijo s čisto BiOBr tetragonalno fazo. Poleg tega je adsorpcijsko-desorpcijska analiza pokazala manjši premer por v vzorcu, pripravljenem pri 145 °C v 18 urah. Reakcijska temperatura močno vpliva na različne lastnosti materiala, ki posledično vplivajo na fotokatalitsko aktivnost.